

Mixture Outlier Exposure for Out-of-Distribution Detection in Fine-Grained Settings

Jingyang Zhang, Nathan Inkawich, Randolph Linderman, Yiran Chen, Hai Li
Duke University

jingyang.zhang@duke.edu

Abstract

Enabling out-of-distribution (OOD) detection for DNNs is critical for their safe and reliable operation in the open world. Despite recent progress, current works often consider a coarse level of granularity in the OOD problem, which fail to approximate many real-world fine-grained tasks where high granularity may be expected between the in-distribution (ID) data and the OOD data (e.g., identifying novel bird species for a bird classification system in the wild). In this work, we start by carefully constructing four large-scale fine-grained test environments in which existing methods are shown to have difficulties. We find that current methods, including ones that include a large/diverse set of outliers during DNN training, have poor coverage over the broad region where fine-grained OOD samples locate. We then propose Mixture Outlier Exposure (MixOE), which effectively expands the covered OOD region by mixing ID data and training outliers, and regularizes the model behaviour by linearly decaying the prediction confidence as the input transitions from ID to OOD. Extensive experiments and analyses demonstrate the effectiveness of MixOE for improving OOD detection in fine-grained settings.

1. Introduction

Out-of-distribution (OOD) detection is the problem of identifying novel data samples during inference time that do not belong to one of the DNN’s known classes. Such detection is crucial for building safe and reliable intelligent systems that operate in the open world. However, OOD detection has proven to be difficult, as deep networks are known to have poor confidence calibration [9] and are often implicitly trained under closed-world assumptions [2]. In recent years, many OOD detection algorithms have been proposed [12, 13, 15, 17, 18, 22, 23, 26, 27, 36], and they have shown to be proficient at detecting rather “obviously OOD” inputs (e.g., detecting when an image of a numerical digit is input into a model that is aware of animals and vehicles).

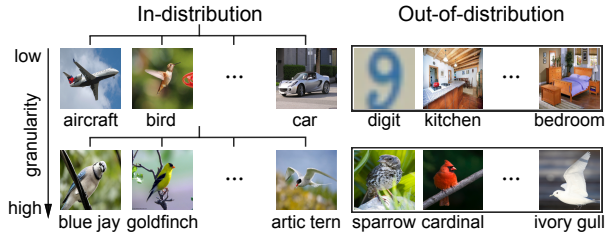


Figure 1. OOD detection in coarse/fine-grained settings.

Despite this progress, we argue that a key limitation in the design and evaluation of many OOD detection methods is the limited scope of *granularity* that is considered. Here, we define granularity as an intuitive measure of the semantic subtlety/nuance between different categories involved in the ID and OOD data. A representative low-granularity task is the most common experiment featured in existing works (Fig. 1 first row), where the coarse-grained CIFAR-10/100 is used as the ID dataset, and the semantically unrelated SVHN and LSUN are used as the OOD datasets [15, 23, 26, 27, 36, 37, 42]. While being simple and convenient to setup, this kind of experiment may not closely approximate many real-world tasks where the OOD data will likely be highly granular (*i.e.*, semantically similar) w.r.t. the ID data. Specifically, in applications such as fine-grained visual classification [14, 45, 48], medical image classification [6, 24], and remote sensing systems [43, 44, 49], one can imagine that a deployed model (*e.g.*, a bird classifier) will encounter not only *coarse-grained* OOD samples (*e.g.*, cars and aircrafts) but also *fine-grained* OOD samples (*e.g.*, unseen bird species, see Fig. 1 second row). Intuitively, fine-grained novel inputs are more difficult to identify due to their semantic/visual similarity to the ID data, which makes OOD detection in fine-grained settings more challenging than those considered in prior works.

Unfortunately, this topic has only been briefly touched by a small number of works [1, 31, 38], where fine-grained settings were used purely for evaluation purpose without being thoroughly studied. Besides, existing works either operated at a rather limited scale, *i.e.*, very few ID classes were considered [1, 38], or made unrealistic practices such as training on a labeled outlier dataset that overlaps with

testing OOD data distribution [31]. The insufficient attention received by this challenging yet realistic topic and the limitations of prior works necessitate 1) a closer investigation and 2) the development of a more reliable methodology for OOD detection in fine-grained settings.

Ultimately, we make three key contributions in this work. First, we build four large-scale fine-grained test environments to approximate real-world complexity and conduct initial evaluations of several state-of-the-art OOD detection methods (Sec. 3). We find that all approaches struggle to detect fine-grained novelties while many of them indeed excel at detecting coarse-grained OOD samples. More surprisingly, most of the “advanced” methods actually underperform a simple softmax confidence thresholding score [12] when facing fine-grained OOD inputs. The initial results highlight the challenging nature of OOD detection when high granularity is involved. Second, we conduct analysis in DNN’s feature space and identify that, in contrast to coarse-grained OOD data which locate in a rather compact region and are relatively far away from ID clusters, fine-grained OOD samples span a broader region and can be much closer to the ID clusters (Sec. 4.1). We also show that the state-of-the-art Outlier Exposure [13], which include a large/diverse set of outlier data during DNN training, fails to provide sufficient coverage over the large OOD region and therefore has little effect on fine-grained OOD data.

The analysis directly motivates our third contribution, *Mixture Outlier Exposure* (MixOE), which is a novel DNN training algorithm for OOD detection in fine-grained settings (Sec. 4.2). Unlike previous OE-based methods [13, 27] that only cover a small OOD region, our methodology aims to induce regularization over a larger OOD area so that it has clear implications for both coarse- and fine-grained OOD samples. Specifically, we propose to perform *mixing operations* (*i.e.*, Mixup [47] or CutMix [46]) between ID data and outlier data to get virtual outlier samples which can be both near to and far away from the ID clusters. The model is then trained in a way such that the prediction confidence linearly decays as the input transitions from ID to OOD. Experimental results on the four test benches show that a simple fine-tuning with MixOE for a few epochs can lead to consistently higher or competitive detection rates against both coarse- and fine-grained OOD data (Sec. 5). We also conduct careful ablation study to further understand why and how MixOE works.

2. Related work

OOD detection approaches. Many popular works in OOD detection research use a pre-trained DNN classifier as a base model, and design an OOD scoring mechanism that leverages some signal from this model. Several methods utilize the output space of the classifier, *e.g.*, MSP [13], ODIN [26], and Energy [27], while other works such as

Mahalanobis detector [23] and Gram Matrices [36] focus on the intermediate feature space of DNNs. Recent works also start to explore the potential of gradient information [16].

Another line of research modifies the base DNN’s training phase to enable better detection. Lee *et al.* [22] proposed to synthesize OOD samples with a GAN [32] and force the classifier to be less confident on the generated OOD data. Hendrycks *et al.* [13] later showed that a diverse and realistic outlier distribution is more proficient than synthetic samples at encouraging low confidence predictions on unseen OOD data. Our work is most closely related to [13] in that we too use an *unlabeled* outlier training set. However, our method uniquely formulates the learning procedure that has explicit consideration of operating in a fine-grained setting where highly granular OOD inputs are expected. We also remark that the above works all consider relatively coarse-grained settings in their experiments.

Mixing operations for OOD detection. Our work also relates to, but differs significantly from a few works that utilized mixing operations in the context of OOD detection. The work of [39] and [4] both empirically evaluated Mixup’s effect on OOD detection. In this work, instead of plainly applying Mixup or CutMix as a regular ID training strategy, we leverage them to construct the virtual outlier distribution to expand the coverage over OOD region. Ravikumar *et al.* [33] proposed to apply Mixup either between ID samples or between the training outliers. In contrast, in our framework the mixing operations are performed between ID and outlier data, which has explicit implication in characterizing the transition from ID to OOD region. In Sec. 5.3, we will demonstrate the superiority of the proposed MixOE over these methods through careful ablation study.

Towards granular OOD detection. As aforementioned, there are a few works that in experimentation made some initial explorations in fine-grained OOD detection, yet they all have significant limitations. In the work of [31], a *labeled* outlier dataset was used for training, which we believe is a prohibitive assumption in reality. Even more concerning, the training outlier dataset used in its experiments (ImageNet [5]) overlapped with the testing OOD data (CUB [41] and Stanford Dogs [20]), which makes the detection (arguably) trivial. The work of [1] and [38] are limited in that the scale of the fine-grained detection problems in their experiments is rather small, *i.e.*, only tens of or even fewer ID classes were considered, whereas we operate at a much larger scale with hundreds of ID classes. Later, we will also show that the method studied in [1] is not yet effective for detecting fine-grained OOD examples.

We also notice some recent works that purposefully consider settings where the test OOD samples are semantically related to the ID classes [19, 42]. The critical difference here is that while we assume high granularity w.r.t. both 1) the ID classes and 2) the “distance” between OOD and ID data,

their considered settings only fit within the second axis of granularity. We argue that this is a crucial distinction because without such ID granularity it may be debatable whether a model *should* be asked to detect granular OOD samples! For example, consider an experiment in [42] that regards “leopard” (in CIFAR-100) as a granular OOD sample for a CIFAR-10 model (which contains a “cat” class). This situation begs the question: given a model trained on cats, is it more desirable to generalize to the notion of a leopard¹, or to identify leopards as OOD? We posit that this is an ill-posed question for a general OOD task because either of the decisions may be correct depending on the application. In this work, since we consider ID classes that are themselves highly granular (*e.g.*, unique bird species), such ambiguity is avoided and the fine-grained novelties (*e.g.* novel bird species) should be considered OOD.

3. Challenges of fine-grained OOD detection

This section describes a detailed study on OOD detection in fine-grained settings and serves to further motivate our goal of improving detection explicitly in fine-grained scenarios. In Sec. 3.1 we describe the construction of the four fine-grained test environments, which is necessary because those presented in prior works are limited in scale. In Sec. 3.2, through initial evaluations we show that fine-grained OOD detection presents distinct challenges for existing methods.

3.1. Test environments

The test environments are curated from four public fine-grained visual classification (FGVC) datasets, namely FGVC-Aircraft [29], Stanford Cars [21], Butterfly [3], and North American Birds [40]. We refer to them as *Aircraft*, *Car*, *Butterfly*, and *Bird*, respectively. For each dataset, we create ID/OOD splits using a holdout class method, *i.e.*, we keep some of the categories as ID and the rest are held out from the training set and considered OOD at test time. To avoid implicit bias that might exist in each single split [1], we randomly produce three ID/OOD splits for each dataset with equal counts of ID/OOD categories. In Tab. 1 we present a comparison between our constructed environments and previous ones. By considering 100+ ID classes we are operating at a larger scale which we believe better represents a wide variety of complex real-world tasks and avoids putting any restrictive assumptions about the complexity of the ID classification task that would make our findings less scalable. We also leave a reasonable number of classes as OOD to reflect the diversity of the open world.

Besides fine-grained novel inputs, a reliable detector in the wild should also be able to identify coarse-grained OOD data. Here, for each dataset, we take the images from the

¹This is actually the desired behaviour in the problem of subpopulation shift robustness [35].

Table 1. Statistics of constructed fine-grained OOD settings.

	# ID classes	# OOD classes
[31]	[100, 60]	[100, 60]
[1]	[11, 9, 8, 7, 7]	[1, 1, 1, 1, 1]
[38]	[46, 20]	[47, 5]
Ours	[200, 150, 150, 90]	[55, 50, 46, 12]

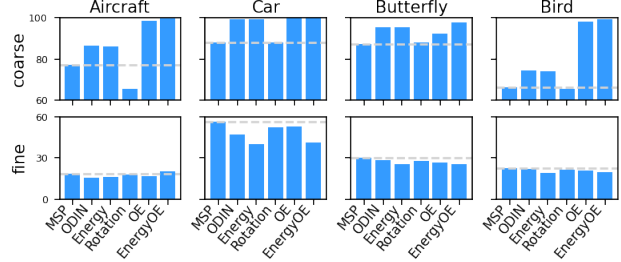


Figure 2. TNR95 statistics of existing methods against coarse-grained (first row) and fine-grained OOD data (second row).

other datasets as coarse-grained OOD samples (*e.g.*, when *Bird* is ID, *Butterfly*, *Car*, and *Aircraft* will be considered OOD). The detection performance is then evaluated against both coarse-grained and fine-grained novelties.

3.2. Evaluating existing methods

Setup. We now evaluate five state-of-the-art detectors in the constructed fine-grained environments, including three post-training scorers² (MSP [12], ODIN [26], and Energy [27]) and two that incorporate training-time regularizations (OE [13] and EnergyOE [27]). In addition, we consider the method Rotation [1] which was studied in a related work that mentioned fine-grained detection. We leave the implementation details of the detection methods to Sec. 5.1 and Appendix A. To measure detector performance, we use two common metrics [15, 22, 23]: true negative rate at a 95% true positive rate (TNR95) and area under the receiver operating characteristic curve (AUROC). While AUROC is a holistic measurement obtained by varying the threshold, TNR95 indicates what portion of OOD samples could be detected when the recall of ID data is 95%. TNR95 is known to better separate different detectors since achieving a high TNR95 is much harder than achieving a high AUROC [15].

Observations. Figure 2 shows the TNR95 results of the evaluation on one of the three splits in each dataset (see Appendix C Fig. 8 for other splits’ results which present similar patterns). Also see the full result table including AUROC statistics in Appendix C Tab. 5. From these results we make two important observations. First, fine-grained OOD samples are significantly more difficult to detect than

²We also evaluated Mahalanobis detector [23] but simply got NaN error, which aligns with [10]’s finding that it can have scalability issue.

coarse-grained ones. Specifically, while most methods can achieve more than around 80% TNR95 when detecting coarse-grained OOD samples (Fig. 2 first row), the TNR95 drops to below 30% for all methods on 3 of the 4 datasets when facing fine-grained OOD (Fig. 2 second row). This observation is in line with recent findings that detection becomes more challenging when OOD data are semantically similar to ID classes [15, 19, 42]. Our second observation is more surprising: on the holdout fine-grained data, even the methods that explicitly include outlier data during the training (OE and EnergyOE) do not reliably outperform MSP, which simply thresholds the softmax prediction confidence and does not have any training-time modifications. This finding directly contrasts the results on coarse-grained data, where more advanced methods consistently outperform MSP. In all, these trends clearly demonstrate that OOD detection in fine-grained settings with highly granular OOD inputs is particularly challenging for existing detectors.

4. Methodology

4.1. Motivating analysis

Before we discuss our training methodology in detail, we first perform two motivational analyses to elucidate the shortcomings of two related methods and to clarify some of the design choices for our method. Notice from Fig. 2 that MSP and OE are generally among the top performers. Both methods operate by thresholding the softmax prediction confidence, and the main difference between the two is in the training of the base DNN classifier. While MSP is applied to a DNN trained in a “standard” way, *i.e.*, by minimizing the average cross-entropy loss over the original ID-only training dataset, OE incorporates extra outlier data to explicitly regularize the model’s confidence on OOD samples (not necessarily from the expected test OOD distribution). Formally, the training objective of OE is formulated as

$$\mathbb{E}_{(x,y) \sim \mathcal{D}_{\text{in}}} [\mathcal{L}(f(x), y)] + \beta \mathbb{E}_{x' \sim \mathcal{D}_{\text{out}}^{\text{OE}}} [\mathcal{L}(f(x'), \mathcal{U})]. \quad (1)$$

Here, \mathcal{D}_{in} is the ID training dataset where (x, y) is a labeled sample, $\mathcal{D}_{\text{out}}^{\text{OE}}$ is the OOD training distribution that is represented by a large and diverse set of unlabeled outlier samples x' , $\mathcal{L}(f(x), y)$ is the cross-entropy loss between the DNN’s predicted distribution $f(x)$ and the ground truth distribution y , \mathcal{U} is the uniform distribution over the ID classes, and β is a weighting term. Essentially, the OE objective encourages a sort of confidence calibration on ID/OOD data, where the predictions on ID samples to be maximally confident (*i.e.*, resemble a one-hot distribution), and the outputs on OOD training samples to have maximum entropy/uncertainty (*i.e.*, resemble a uniform distribution).

Prediction confidences. We first monitor the prediction confidence of the Standard and OE models on ID/OOD samples, which allows us to more clearly see how they are “inter-

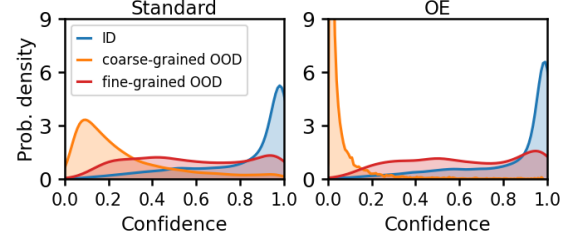


Figure 3. Confidence density plot of the Standard and OE model.

preting” the data beyond the high-level detection statistics described in Sec. 3.2. Figure 3 visualizes the distributions of prediction confidence measured on one split from the *Bird* dataset (see Appendix C Figs. 9 to 12 for results on other splits/datasets). Our main takeaway here is that while OE indeed helps the model yield lower confidence predictions when facing coarse-grained OOD data, it does not have the same effect on the fine-grained data. Rather, the fine-grained confidence distribution for the OE model is very similar to that of the Standard model, which directly explains the very similar fine-grained performance in Fig. 2.

Feature space analysis. To further understand why OE fails to improve fine-grained OOD, we measure the distance between ID and OOD data in the feature space of a DNN model. Specifically, we visualize the ID/OOD sample features extracted by the Standard model (the outputs of the penultimate layer) together in a 2D space. The details of the visualization procedure are described in Appendix B. Figure 4 shows the results on the *Car* dataset (see Appendix C Figs. 13 to 16 for plots on other datasets), from which we make two key observations. First, as shown in Fig. 4 (b), coarse-grained OOD data locate in a rather compact region, with a small portion of samples intersecting with one of the ID cluster and others being relatively far away from the ID region. According to Fig. 4 (c), however, fine-grained OOD samples span a much broader area, with many of them being very close to or even within the ID clusters, due to their semantic similarity to the ID images. This observation reinforces the TNR95 detection results in Fig. 2, where fine-grained novelties are significantly more difficult to detect than coarse-grained ones.

Second, according to Fig. 4 (d), the OE’s training outlier data span a rather small area which “enclose” the coarse OOD data region but fail to cover the larger area where many fine-grained OOD data locate. This observation explains OE’s vast improvements in coarse-grained detection and the limited effect in fine-grained detection. We note that this problem is not likely to result from the insufficient diversity of the outlier dataset, as the one used here already includes more than 700 classes [25]. One may also wonder what if the outlier set contains some fine-grained outlier data. However, we do not want to assume that one would have a large/diverse set of fine-grained outliers for training, which is also a key

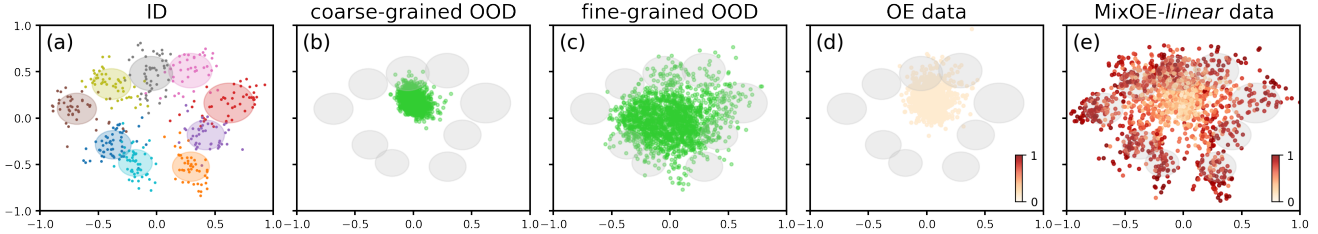


Figure 4. 2D visualization of ID/OOD/training outlier data in the feature space. The circles stand for ID clusters. The color lightness in (d) and (e) indicates the confidence encoded in the soft target, where darker color corresponds to higher confidence. Note, the number of data points used in the plot is the same across (b), (c), (d), (e).

of OE in general where the outlier set does not necessarily contain the expected test OOD data, and people are going for “generalization” to novel forms of OOD instead of trivially “overfitting” to a certain types of OOD. In summary, we have now exposed the problem that vanilla OE fails to provide sufficient coverage over the broad region where fine-grained OOD samples locate and therefore rarely improves the fine-grained detection.

4.2. Mixture Outlier Exposure

To explicitly regularize the model’s behaviour in a broader region to improve detection against both coarse- and fine-grained OOD data, we propose Mixture Outlier Exposure (MixOE), whose high-level objective is formulated as

$$\mathbb{E}_{(x,y) \sim \mathcal{D}_{\text{in}}} [\mathcal{L}(f(x), y)] + \beta \mathbb{E}_{(\tilde{x}, \tilde{y}) \sim \mathcal{D}_{\text{out}}^{\text{virtual}}} [\mathcal{L}(f(\tilde{x}), \tilde{y})]. \quad (2)$$

The key concept of MixOE is to create a “virtual” outlier distribution which can provide a more comprehensive coverage over the OOD region than the empirical $\mathcal{D}_{\text{out}}^{\text{OE}}$. The intuition directly comes from Fig. 4: If we “interpolate” the ID samples (Fig. 4 (a)) and outlier data (Fig. 4 (d)), the resulting samples are likely to span a larger area and cover the fine-grained OOD data (Fig. 4 (c)). To this end, we construct $\mathcal{D}_{\text{out}}^{\text{virtual}}$ with virtual training samples \tilde{x} which are obtained by interpolating/mixing samples from \mathcal{D}_{in} and $\mathcal{D}_{\text{out}}^{\text{OE}}$, *i.e.*, $\tilde{x} = \text{mix}(x_{\text{in}}, x_{\text{out}}^{\text{OE}}, \lambda)$. Here, $x_{\text{in}} \sim \mathcal{D}_{\text{in}}$, $x_{\text{out}}^{\text{OE}} \sim \mathcal{D}_{\text{out}}^{\text{OE}}$, $\text{mix}(\cdot, \cdot, \cdot)$ is a mixing function, and λ is a coefficient that controls the weighting of the two source images x_{in} and $x_{\text{out}}^{\text{OE}}$. In this work, we use the well-established mixing operations Mixup [47] (*linear* mixing) and CutMix [46] (*cut* mixing) as the mixing function, and let λ to be sampled from a Beta distribution $\text{Beta}(\alpha, \alpha)$ at each training iteration for an introduced hyperparameter α . To demonstrate the effect of mixed samples \tilde{x} , we again visualize them in the DNN model’s feature space in Fig. 4 (e) (here we use *linear* mixing as an example; see Appendix C Figs. 13 to 16 for more). Importantly, unlike the empirical outlier distribution $\mathcal{D}_{\text{out}}^{\text{OE}}$ in Fig. 4 (d), our virtual outlier samples can span a larger area (being *both* near to and far away from the ID clusters) by varying the coefficient λ . As a result, we anticipate that when train-

ing with the samples from $\mathcal{D}_{\text{out}}^{\text{virtual}}$, the model’s behaviour on both fine- and coarse-grained OOD data can be regularized.

Another key difference between MixOE and OE resides in the soft targets that are assigned to the training outliers. Recall that in vanilla OE all the outliers should be “predicted” as a uniform distribution \mathcal{U} , *i.e.*, the model should be minimally confident on the outlier data. In MixOE, however, naively forcing the lowest confidence on all outliers is not reasonable as they can be either close to or far away from the ID clusters. For example, in an extreme case where the mixed sample weights the ID image by 0.99 and the outlier image by 0.01, forcing the model to output uniform distribution is very likely to prevent it from learning useful information. Therefore, we opt to generate soft targets \tilde{y} by linearly interpolating the one-hot label y_{in} (corresponding to x_{in}) and the uniform distribution (corresponding to $x_{\text{out}}^{\text{OE}}$) according to λ , *i.e.*, $\tilde{y} = \lambda y_{\text{in}} + (1 - \lambda)\mathcal{U}$. With such soft targets, the MixOE objective can be interpreted as explicitly controlling how the DNN’s prediction confidence decays as the input image transitions between ID and “far-away” OOD samples. A visualization of such effect can be seen in Fig. 4 (e), where darker points correspond to a higher confidence that is encoded in their soft targets \tilde{y} . Similar to OE, after training the detection will be performed by thresholding the prediction confidence, and we anticipate that MixOE will lead to more moderate confidence estimates on fine-grained OOD inputs.

5. Experiments

5.1. Setup

Baselines. We consider a total of seven baseline methods. Six of them are the same as Sec. 3.2, including five state-of-the-art methods [12, 13, 26, 27] and one that was studied in a previous fine-grained setting [1]. We further consider Corruption [37], which creates training outlier data by distorting the ID images with different types of corruptions and various level of intensities [11]. Similar to our MixOE, we find that Corruption has the potential to cover a broader OOD region and thus it is included as a baseline.

Training. For the post-training scoring methods, we train

ResNet-50 models [8] in the standard fashion, *i.e.*, by minimizing the cross-entropy loss over the ID-only training dataset. Specifically, we train the model for 90 epochs using SGD with the batch size being 32. Following common practices in fine-grained classification research [14, 45, 48], the model is initialized with ImageNet pre-trained weights. The initial learning rate is 0.001 and is decayed by cosine learning rate schedule [28]. For Rotation and Corruption, we train the model using their corresponding objective with the same setup as the standard training.

For OE-based methods, we only fine-tune the trained standard model with OE/EnergyOE/MixOE objective for 10 epochs, following [13, 27]. The fine-tuning also adopts cosine schedule with the initial learning rate being 0.001. The batch size of ID data is still 32. For OE and EnergyOE, as suggested in their papers, we set the batch size of outlier data to be twice as the ID batch size, which is 64. In the case of MixOE, we keep outlier batch size same as the ID batch size. The outlier training set $\mathcal{D}_{\text{out}}^{\text{OE}}$ we consider for these methods is WebVision 1.0 [25], which contains natural images simply crawled from Flickr and Google by querying with the 1,000 categories of ImageNet. We believe this dataset represents a realistic construction of $\mathcal{D}_{\text{out}}^{\text{OE}}$ for many ID tasks in the natural imagery domain. Importantly, to avoid arguments of “cheating” we filter out images relevant to the considered OOD tasks from $\mathcal{D}_{\text{out}}^{\text{OE}}$, *i.e.*, all aircraft, car, butterfly, and bird images are removed.

Hyperparameter tuning. We take great care to ensure that the hyperparameter tuning is fair. First, we randomly holdout a portion of samples from the ID training set as validation data to avoid directly tuning on ID test data. Second, we randomly select samples from the training outlier set $\mathcal{D}_{\text{out}}^{\text{OE}}$ to serve as OOD validation data. Although non-OE-based methods do not assume the availability of an outlier dataset, for the fairness of comparison we use the same group of OOD validation data for all methods. Critically, note that the OOD validation data reveals no information about the test-time OOD distribution since we already filter out all relevant images from $\mathcal{D}_{\text{out}}^{\text{OE}}$.

With the selected ID and OOD validation samples, we tune the hyperparameters such that the OOD detection performance is maximized and the ID classification accuracy is minimally affected. To test the method robustness, in each of the four environments we only tune the hyperparameter once for each approach using a single split; the determined hyperparameter is then applied to all splits from the same dataset. In Appendix A we present a detailed list of the candidate hyperparameter values and the final determined values we use for each method in our experiments.

Evaluation. The evaluation procedure follows the one described in Sec. 3.1 and Sec. 3.2. For each dataset, we consider the holdout classes as fine-grained OOD data and the samples from other datasets as coarse-grained OOD data.

Table 2. Detection performance in terms of TNR95 statistics. The number before and after the slash is for coarse-grained and fine-grained OOD samples, respectively. Avg. diff. is the average difference (across three splits) relative to MSP.

\mathcal{D}_{in}	Method	Split 1	Split 2	Split 3	Avg. diff.
Aircraft	MSP [12]	75.0 / 29.9	61.6 / 15.9	77.1 / 18.5	- / -
	ODIN [26]	87.5 / 30.2	73.2 / 15.3	86.5 / 15.8	+11.2 / -1.0
	Energy [27]	88.5 / 30.1	74.4 / 14.6	86.2 / 16.3	+11.8 / -1.1
	Rotation [1]	65.5 / 31.4	55.0 / 15.9	65.5 / 17.6	-9.2 / +0.2
	Corruption [37]	95.9 / 33.2	94.2 / 20.1	95.6 / 19.4	+24.0 / +2.8
	OE [13]	99.3 / 27.8	98.5 / 16.0	98.7 / 16.5	+27.6 / -1.3
	EnergyOE [27]	99.8 / 30.3	99.7 / 17.0	99.7 / 19.9	+28.5 / +1.0
	MixOE-linear	93.2 / 41.4	88.4 / 24.6	92.1 / 16.5	+20.0 / +6.1
	MixOE-cut	99.0 / 39.8	99.4 / 23.7	99.4 / 24.9	+28.0 / +8.0
	MSP [12]	95.5 / 58.5	88.0 / 56.3	78.8 / 53.5	- / -
Car	ODIN [26]	99.6 / 55.6	99.1 / 47.0	97.8 / 49.0	+11.4 / -5.6
	Energy [27]	99.7 / 49.1	99.4 / 39.7	99.1 / 42.6	+12.0 / -12.3
	Rotation [1]	97.7 / 58.9	88.1 / 52.4	81.3 / 50.4	+1.6 / -2.2
	Corruption [37]	99.5 / 63.0	99.2 / 55.5	98.2 / 60.0	+11.5 / +3.4
	OE [13]	99.9 / 53.2	100.0 / 53.0	99.9 / 51.2	+12.5 / -3.6
	EnergyOE [27]	100.0 / 52.6	100.0 / 41.0	100.0 / 44.9	+12.6 / -9.9
	MixOE-linear	99.6 / 65.9	99.7 / 62.9	99.5 / 60.1	+12.2 / +6.9
	MixOE-cut	99.9 / 70.3	100.0 / 69.8	99.9 / 66.5	+12.5 / +12.8
	MSP [12]	87.1 / 29.9	89.9 / 31.8	88.4 / 36.6	- / -
	ODIN [26]	95.2 / 28.2	95.5 / 32.5	95.6 / 38.7	+7.0 / +0.4
Butterfly	Energy [27]	95.3 / 25.5	95.2 / 30.2	95.6 / 36.1	+6.9 / -2.2
	Rotation [1]	87.9 / 27.6	88.5 / 31.2	86.2 / 37.0	-0.9 / -0.8
	Corruption [37]	94.1 / 29.0	94.2 / 32.9	92.1 / 38.0	+5.0 / +0.5
	OE [13]	92.2 / 26.5	93.7 / 32.1	94.3 / 34.3	+4.9 / -1.8
	EnergyOE [27]	97.8 / 25.1	96.9 / 30.5	98.2 / 37.2	+9.2 / -1.8
	MixOE-linear	95.3 / 32.6	93.9 / 37.9	95.5 / 45.0	+6.4 / +5.7
	MixOE-cut	94.9 / 35.8	94.1 / 38.8	92.7 / 46.0	+5.4 / +7.4
	MSP [12]	72.3 / 22.6	67.4 / 22.3	66.4 / 22.3	- / -
	ODIN [26]	80.9 / 22.7	77.2 / 21.5	74.3 / 21.9	+8.8 / -0.4
	Energy [27]	80.8 / 20.3	76.5 / 18.4	73.9 / 18.8	+8.4 / -3.2
Bird	Rotation [1]	71.3 / 23.6	64.0 / 24.0	65.4 / 21.5	-1.8 / +0.6
	Corruption [37]	81.1 / 23.2	81.8 / 23.7	83.9 / 26.6	+13.6 / +2.1
	OE [13]	98.2 / 20.6	97.9 / 22.9	97.9 / 20.7	+29.3 / -1.0
	EnergyOE [27]	98.6 / 19.4	99.0 / 18.4	99.3 / 19.5	+30.3 / -3.3
	MixOE-linear	88.6 / 24.9	83.9 / 26.7	86.3 / 28.6	+17.6 / +4.3
	MixOE-cut	91.0 / 27.7	91.8 / 24.6	92.9 / 27.7	+23.2 / +4.3

Following [15, 22, 23], we consider ID as positive and OOD as negative, and use TNR95 and AUROC as the metrics.

5.2. Results

Detection performance. Table 2 shows the TNR95 results across the four test benches. The AUROC statistics yield similar patterns to TNR95 and are left in the expanded Tab. 5 in Appendix C. Our first observation is that MixOE consistently achieves the best detection performance against fine-grained OOD samples. Specifically, averaged across the three splits on the [Aircraft, Car, Butterfly, Bird] tasks, MixOE-linear and MixOE-cut improve the TNR95 over MSP by [+6.1%, +6.9%, +5.7%, +4.3%] and [+8.0%, +12.8%, +7.4%, +4.3%], respectively. In comparison, the vanilla OE’s relative improvement over MSP is [-1.3%, -3.6%, -1.8%, -1.0%]. Similar to OE, most of the baseline methods do not provide consistent or noticeable gains in fine-grained OOD TNR95 across the four datasets either. We also remark that MixOE-linear and MixOE-cut both lead to significant improvements, demonstrating that the validity of the general idea behind

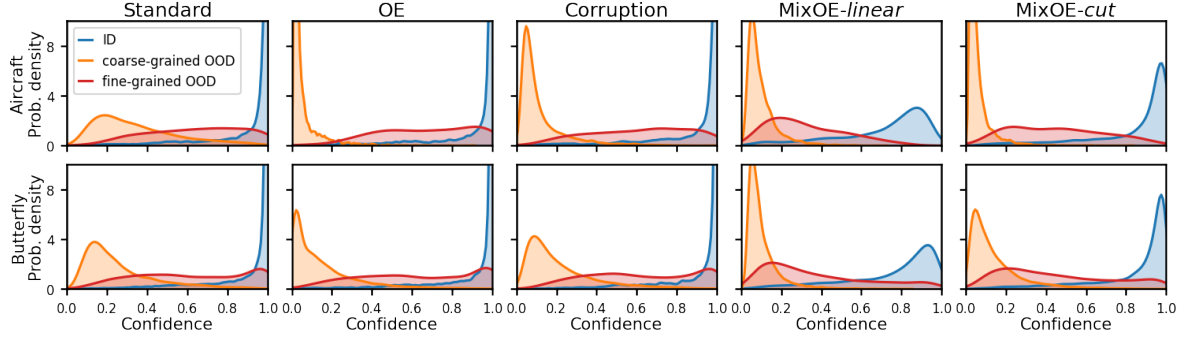


Figure 5. Confidence density plots for different methods on the *Aircraft* and *Butterfly* dataset.

MixOE is independent of the specific mixing operations being used.

Our second observation is that MixOE can perform on par with state-of-the-art methods in detecting coarse-grained OOD samples. On the four tasks MixOE-*linear* and MixOE-*cut* improve the TNR95 over MSP by [+20.0%, +12.2%, +6.4%, +17.6%] and [+28.0%, +12.5%, +5.4%, +23.2%], respectively. OE, whose effect is exclusively towards coarse-grained OOD data, leads to improvements of [+27.6%, +12.5%, +4.9%, +29.3%]. Overall, these evaluation results display the effectiveness of MixOE in enabling better detection performance against both fine- and coarse-grained OOD data.

Finally, we comment on the method performance when considering both types of OOD samples together. We notice that except our proposed MixOE, Corruption is the only baseline method that consistently improves upon MSP against both fine- and coarse-grained novelties across all the datasets, which is reasonable because both methods regularize a larger area in the OOD region (see Sec. 5.3 for a detailed discussion). Yet, Corruption’s performance still does not match that of MixOE: For example, the relative improvement of MixOE-*cut* over Corruption against fine- and coarse-grained data is [+5.2%, +9.4%, +6.9%, +2.2%] and [+4.0%, +1.0%, +0.4%, +9.6%], respectively.

Prediction confidences. To more closely understand how MixOE improves the OOD detection in fine-grained settings, we again monitor the confidence distributions of the models on ID/OOD samples. Figure 5 shows the confidence density plots of Standard, OE, Corruption and MixOE models on one of the splits from the *Aircraft* and *Butterfly* dataset (see Appendix C Figs. 9 to 12 for more). From Fig. 9 we can clearly identify that, regardless of the mixing operation, the MixOE models consistently produce lower confidence predictions on fine-grained OOD samples, making them more distinguishable from ID inputs. This observation confirms that the virtual outlier data and their corresponding soft targets introduced in MixOE indeed help regularize the model’s outputs on fine-grained OOD samples.

ID classification accuracy. Lastly, we examine how the

Table 3. Accuracy comparison of the training algorithms. The numbers in the parenthesis are the differences relative to the accuracy of standard training. Avg. diff. shows the improvements averaged across the four datasets.

	Aircraft	Car	Butterfly	Bird	Avg. diff.
Rotation [1]	88.5 (-1.1)	91.3 (-0.6)	88.8 (-0.1)	82.0 (-0.1)	-0.5
Corruption [37]	89.8 (+0.2)	92.4 (+0.6)	89.6 (+0.6)	83.7 (+1.6)	+0.8
OE [13]	89.2 (-0.5)	91.6 (-0.2)	88.1 (-0.9)	82.4 (+0.3)	-0.3
EnergyOE [27]	89.3 (-0.3)	91.8 (-0.0)	88.8 (-0.2)	82.3 (+0.2)	-0.1
MixOE- <i>linear</i>	90.5 (+0.8)	92.9 (+1.1)	89.3 (+0.3)	83.4 (+1.3)	+0.9
MixOE- <i>cut</i>	90.1 (+0.5)	92.9 (+1.1)	90.1 (+1.2)	83.5 (+1.4)	+1.1

training methods can affect the ID classification accuracy because we do not intend to tradeoff accuracy for detection performance. In Tab. 3 we show the accuracy on each dataset averaged across the three splits (see Appendix C Tab. 6 for unaveraged results). Interestingly, unlike other training strategies, Corruption and our MixOE-*linear*/MixOE-*cut* can improve the accuracy by 0.8%, 0.9%, and 1.1% on average across the four environments, respectively. Our hypothesis here is that since the fine-grained datasets often have relatively small number of training samples (*e.g.*, tens of images per class), some of the training “outliers” generated by MixOE or Corruption that are close to the ID clusters actually serve as augmented data and thus contribute to the ID accuracy.

5.3. Ablation study

MixOE v.s. Mix. Recall that the core idea of MixOE is to mix ID and outlier data for DNN training. In Sec. 5.2 we have shown that this concept is more beneficial than using the outlier data alone without mixing (vanilla OE). Here we ablate MixOE along another direction: We contrast MixOE with vanilla Mix training which does not use the auxiliary outlier data, *i.e.*, mixing only ID data. Concretely, for Mix training the generation of virtual outlier samples in Eq. (2) is changed to $(\tilde{x}, \tilde{y}) = (\text{mix}(x_1, x_2, \lambda), \lambda y_1 + (1 - \lambda)y_2)$, where $(x_1, y_1), (x_2, y_2) \sim \mathcal{D}_{\text{in}}$. The hyperparameter tuning procedure and training setup is the same as those for MixOE.

The comparison is presented in Fig. 6, where we show the two methods’ average improvements in TNR95 relative to

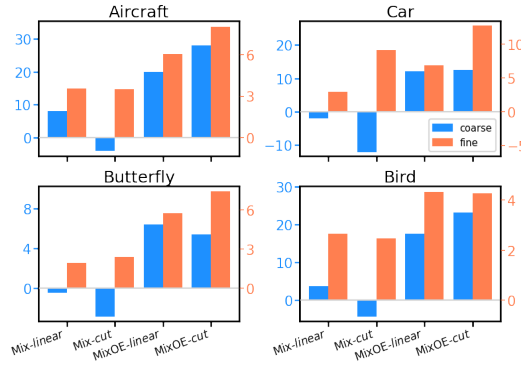


Figure 6. Comparison between MixOE and vanilla Mix training in terms of average difference in TNR95 relative to MSP.

the baseline MSP across the three splits on each dataset. We find that Mix training is able to provide performance gains in detecting fine-grained OOD data, but the gains are smaller than those brought by MixOE; meanwhile, Mix training rarely improves the coarse-grained OOD detection rates.

To explain these results, in Fig. 7 (a) and (b) we visualize the training data used by Mix training in the feature space of a standard-trained model (again, the *Car* dataset is shown here; see Appendix C Figs. 13, 14 and 16 for more). Similar to MixOE, Mix training’s data can also cover a broader space of the OOD region, which accounts for their improved performance against fine-grained OOD data. However, one problem we notice is that the confidence encoded in the soft targets of Mix training is still relatively high (above 50%) even when the corresponding inputs are already far away from the ID clusters. This is because when interpolating between two one-hot labels the minimum confidence that can be achieved is 50%. Consequently, during Mix training the prediction confidence of the OOD samples that are relatively far away from the ID clusters may not be pushed towards the lowest level (*i.e.*, resembling uniform distribution as in MixOE, *cf.* Fig. 4 (e)), which can be confirmed by the confidence distribution plots in Appendix C Figs. 9 to 12. This reasoning explains why Mix training underperforms MixOE (especially its little effect on coarse OOD data) and further validates MixOE’s idea of using ID and outlier data together to regularize the prediction confidence over the OOD region.

MixOE v.s. Mix + OE. Upon the previous discussion, one may wonder if naively combining the Mix and OE objective together can achieve similar effect to MixOE. Yet, a crucial problem with such combination is that, while the mixed samples generated by Mix training can overlap with some of the outlier data (compare Fig. 7 (a)/(b) and Fig. 4 (d)), their corresponding soft targets are very different: mixed samples are coupled with “two-hot” targets that result from the interpolation between two one-hot labels, yet OE’s outlier data are trained to match uniform distribution. This incon-

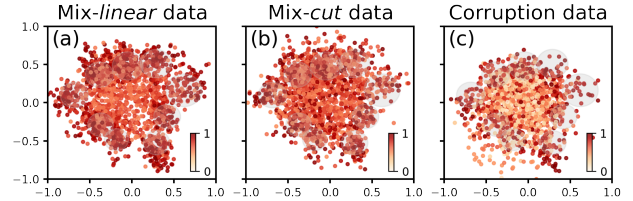


Figure 7. 2D visualization of the ID/OOD/training outlier data in the feature space. The same dataset is used as in Fig. 4. The red color lightness indicates the confidence encoded in the soft target, where darker color corresponds to higher confidence.

sistency is similar to the problem of manifold intrusion [7] and may cause learning difficulty for the model. Indeed, we experimentally find that when combining Mix and OE together, the model’s accuracy can decrease by up to 10%, and the TNR95 can be worse than MSP by 10% and 20% against coarse- and fine-grained OOD samples, respectively. Therefore, the proposed MixOE cannot be replaced by the simple combination of two existing objectives.

MixOE v.s. Corruption. Previously we show that Corruption is another method (besides our MixOE) that consistently enables better detection against both coarse- and fine-grained OOD samples. According to the visualization in Fig. 7 (c), we believe the effectiveness of Corruption can be attributed to that its training outlier data (corrupted ID samples) provide a certain level of coverage over the OOD region, which actually further validate our high-level idea of regularizing a broader area of the OOD space. With that being said, one problem with Corruption which we identify from Fig. 7 is that the confidence assigned to a corrupted ID image may not align with the distance between that sample to the ID clusters (we refer readers to [37] for details on how the soft targets are produced for Corruption). In contrast, our MixOE provides a more explicit and consistent training environment where the confidence decays as the input transitions from ID to OOD. Such difference potentially explains the superior results of MixOE over Corruption as discussed in Sec. 5.2.

6. Conclusion

In this work, we propose Mixture Outlier Exposure, a DNN training algorithm for OOD detection in fine-grained settings. MixOE explicitly addresses vanilla OE’s poor coverage over the broad OOD region by mixing ID data and training outlier samples, and the mixed samples are used to regularize the model’s behaviour such that the prediction confidence linearly decays when the inputs transition from ID to OOD. Experimental results in the four newly built large-scale fine-grained environments demonstrate that MixOE is able to improve the TNR95 by up to 28% and 13% against coarse- and fine-grained OOD data, respectively. We hope that this work will inspire and facilitate future research on OOD detection in the challenging fine-grained settings.

References

[1] Faruk Ahmed and Aaron Courville. Detecting semantic anomalies. In *Proceedings of the AAAI Conference on Artificial Intelligence*, volume 34, pages 3154–3162, 2020. [1](#), [2](#), [3](#), [5](#), [6](#), [7](#), [11](#), [12](#), [19](#)

[2] Abhijit Bendale and Terrance E. Boult. Towards open set deep networks. In *CVPR*, pages 1563–1572. IEEE Computer Society, 2016. [1](#)

[3] Tianshui Chen, Wenxi Wu, Yuefang Gao, Le Dong, Xiaonan Luo, and Liang Lin. Fine-grained representation learning and recognition by exploiting hierarchical semantic embedding. In *Proceedings of the 26th ACM international conference on Multimedia*, pages 2023–2031, 2018. [3](#)

[4] Sanghyuk Chun, Seong Joon Oh, Sangdoo Yun, Dongyoon Han, Junsuk Choe, and Youngjoon Yoo. An empirical evaluation on robustness and uncertainty of regularization methods. *arXiv preprint arXiv:2003.03879*, 2020. [2](#)

[5] Jia Deng, Wei Dong, Richard Socher, Li-Jia Li, Kai Li, and Li Fei-Fei. Imagenet: A large-scale hierarchical image database. In *2009 IEEE conference on computer vision and pattern recognition*, pages 248–255. Ieee, 2009. [2](#)

[6] Mengran Fan, Tapabrata Chakraborti, I Eric, Chao Chang, Yan Xu, and Jens Rittscher. Microscopic fine-grained instance classification through deep attention. In *International Conference on Medical Image Computing and Computer-Assisted Intervention*, pages 490–499. Springer, 2020. [1](#)

[7] Hongyu Guo, Yongyi Mao, and Richong Zhang. Mixup as locally linear out-of-manifold regularization. In *Proceedings of the AAAI Conference on Artificial Intelligence*, volume 33, pages 3714–3722, 2019. [8](#)

[8] Kaiming He, Xiangyu Zhang, Shaoqing Ren, and Jian Sun. Deep residual learning for image recognition. In *Proceedings of the IEEE conference on computer vision and pattern recognition*, pages 770–778, 2016. [6](#)

[9] Matthias Hein, Maksym Andriushchenko, and Julian Bitterwolf. Why relu networks yield high-confidence predictions far away from the training data and how to mitigate the problem. In *Proceedings of the IEEE/CVF Conference on Computer Vision and Pattern Recognition*, pages 41–50, 2019. [1](#)

[10] Dan Hendrycks, Steven Basart, Mantas Mazeika, Mohammadreza Mostajabi, Jacob Steinhardt, and Dawn Song. Scaling out-of-distribution detection for real-world settings. *arXiv preprint arXiv:1911.11132*, 2019. [3](#)

[11] Dan Hendrycks and Thomas Dietterich. Benchmarking neural network robustness to common corruptions and perturbations. *Proceedings of the International Conference on Learning Representations*, 2019. [5](#)

[12] Dan Hendrycks and Kevin Gimpel. A baseline for detecting misclassified and out-of-distribution examples in neural networks. In *International Conference on Learning Representations*, 2017. [1](#), [2](#), [3](#), [5](#), [6](#), [12](#)

[13] Dan Hendrycks, Mantas Mazeika, and Thomas Dietterich. Deep anomaly detection with outlier exposure. In *International Conference on Learning Representations*, 2018. [1](#), [2](#), [3](#), [5](#), [6](#), [7](#), [11](#), [12](#), [19](#)

[14] Yen-Chi Hsu, Cheng-Yao Hong, Ding-Jie Chen, Ming-Sui Lee, Davi Geiger, and Tyng-Luh Liu. Fine-grained visual recognition with batch confusion norm. *arXiv preprint arXiv:1910.12423*, 2019. [1](#), [6](#)

[15] Yen-Chang Hsu, Yilin Shen, Hongxia Jin, and Zsolt Kira. Generalized odin: Detecting out-of-distribution image without learning from out-of-distribution data. In *Proceedings of the IEEE/CVF Conference on Computer Vision and Pattern Recognition*, pages 10951–10960, 2020. [1](#), [3](#), [4](#), [6](#), [11](#)

[16] Rui Huang, Andrew Geng, and Yixuan Li. On the importance of gradients for detecting distributional shifts in the wild. *arXiv preprint arXiv:2110.00218*, 2021. [2](#)

[17] Rui Huang and Yixuan Li. MOS: towards scaling out-of-distribution detection for large semantic space. In *CVPR*, pages 8710–8719, 2021. [1](#)

[18] Nathan Inkawich, Eric Davis, Matthew Inkawich, Uttam Majumder, and Yiran Chen. Training sar-atr models for reliable operation in open-world environments. *IEEE Journal of Selected Topics in Applied Earth Observations and Remote Sensing*, 14:3954–3966, 2021. [1](#)

[19] Ramneet Kaur, Susmit Jha, Anirban Roy, Oleg Sokolsky, and Insup Lee. Are all outliers alike? on understanding the diversity of outliers for detecting oods. *arXiv preprint arXiv:2103.12628*, 2021. [2](#), [4](#)

[20] Aditya Khosla, Nityananda Jayadevaprakash, Bangpeng Yao, and Fei-Fei Li. Novel dataset for fine-grained image categorization: Stanford dogs. In *Proc. CVPR Workshop on Fine-Grained Visual Categorization (FGVC)*, volume 2. Citeseer, 2011. [2](#)

[21] Jonathan Krause, Michael Stark, Jia Deng, and Li Fei-Fei. 3d object representations for fine-grained categorization. In *4th International IEEE Workshop on 3D Representation and Recognition (3dRR-13)*, Sydney, Australia, 2013. [3](#)

[22] Kimin Lee, Honglak Lee, Kibok Lee, and Jinwoo Shin. Training confidence-calibrated classifiers for detecting out-of-distribution samples. In *International Conference on Learning Representations*, 2018. [1](#), [2](#), [3](#), [6](#)

[23] Kimin Lee, Kibok Lee, Honglak Lee, and Jinwoo Shin. A simple unified framework for detecting out-of-distribution samples and adversarial attacks. In *NeurIPS*, 2018. [1](#), [2](#), [3](#), [6](#)

[24] Qing Li, Weidong Cai, Xiaogang Wang, Yun Zhou, David Da-gan Feng, and Mei Chen. Medical image classification with convolutional neural network. In *2014 13th international conference on control automation robotics & vision (ICARCV)*, pages 844–848. IEEE, 2014. [1](#)

[25] Wen Li, Limin Wang, Wei Li, Eirikur Agustsson, and Luc Van Gool. Webvision database: Visual learning and understanding from web data. *arXiv preprint arXiv:1708.02862*, 2017. [4](#), [6](#)

[26] Shiyu Liang, Yixuan Li, and R Srikant. Enhancing the reliability of out-of-distribution image detection in neural networks. In *International Conference on Learning Representations*, 2018. [1](#), [2](#), [3](#), [5](#), [6](#), [11](#), [12](#)

[27] Weitang Liu, Xiaoyun Wang, John Owens, and Yixuan Li. Energy-based out-of-distribution detection. *Advances in Neural Information Processing Systems*, 33, 2020. [1](#), [2](#), [3](#), [5](#), [6](#), [7](#), [11](#), [12](#), [19](#)

[28] Ilya Loshchilov and Frank Hutter. Sgdr: Stochastic gradient descent with warm restarts. *arXiv preprint arXiv:1608.03983*, 2016. [6](#)

[29] S. Maji, J. Kannala, E. Rahtu, M. Blaschko, and A. Vedaldi. Fine-grained visual classification of aircraft. Technical report, 2013. 3

[30] Tianyu Pang, Kun Xu, Yinpeng Dong, Chao Du, Ning Chen, and Jun Zhu. Rethinking softmax cross-entropy loss for adversarial robustness. In *International Conference on Learning Representations*, 2019. 11

[31] Pramuditha Perera and Vishal M Patel. Deep transfer learning for multiple class novelty detection. In *Proceedings of the IEEE/CVF Conference on Computer Vision and Pattern Recognition*, pages 11544–11552, 2019. 1, 2, 3

[32] Alec Radford, Luke Metz, and Soumith Chintala. Unsupervised representation learning with deep convolutional generative adversarial networks. *arXiv preprint arXiv:1511.06434*, 2015. 2

[33] Deepak Ravikumar, Sangamesh Kodge, Isha Garg, and Kaushik Roy. Exploring vicinal risk minimization for lightweight out-of-distribution detection. *arXiv preprint arXiv:2012.08398*, 2020. 2

[34] Ryne Roady, Tyler L Hayes, Ronald Kemker, Ayesha Gonzales, and Christopher Kanan. Are open set classification methods effective on large-scale datasets? *Plos one*, 15(9):e0238302, 2020. 11

[35] Shibani Santurkar, Dimitris Tsipras, and Aleksander Madry. {BREEDS}: Benchmarks for subpopulation shift. In *International Conference on Learning Representations*, 2021. 3

[36] Chandramouli Shama Sastry and Sageev Oore. Detecting out-of-distribution examples with gram matrices. In *International Conference on Machine Learning*, pages 8491–8501. PMLR, 2020. 1, 2

[37] Engkarat Techapanurak, Anh-Chuong Dang, and Takayuki Okatani. Bridging in-and out-of-distribution samples for their better discriminability. *arXiv preprint arXiv:2101.02500*, 2021. 1, 5, 6, 7, 8, 11, 12, 19

[38] Engkarat Techapanurak and Takayuki Okatani. Practical evaluation of out-of-distribution detection methods for image classification. *arXiv preprint arXiv:2101.02447*, 2021. 1, 2, 3

[39] Sunil Thulasidasan, Gopinath Chennupati, Jeff A Bilmes, Tammo Bhattacharya, and Sarah Michalak. On mixup training: Improved calibration and predictive uncertainty for deep neural networks. In H. Wallach, H. Larochelle, A. Beygelzimer, F. d'Alché-Buc, E. Fox, and R. Garnett, editors, *Advances in Neural Information Processing Systems*, volume 32. Curran Associates, Inc., 2019. 2

[40] Grant Van Horn, Steve Branson, Ryan Farrell, Scott Haber, Jessie Barry, Panos Ipeirotis, Pietro Perona, and Serge Belongie. Building a bird recognition app and large scale dataset with citizen scientists: The fine print in fine-grained dataset collection. In *Proceedings of the IEEE Conference on Computer Vision and Pattern Recognition*, pages 595–604, 2015. 3

[41] C. Wah, S. Branson, P. Welinder, P. Perona, and S. Belongie. The Caltech-UCSD Birds-200-2011 Dataset. Technical Report CNS-TR-2011-001, California Institute of Technology, 2011. 2

[42] Jim Winkens, Rudy Bunel, Abhijit Guha Roy, Robert Stanforth, Vivek Natarajan, Joseph R Ledsam, Patricia MacWilliams, Pushmeet Kohli, Alan Karthikesalingam, Simon Kohl, et al. Contrastive training for improved out-of-distribution detection. *arXiv preprint arXiv:2007.05566*, 2020. 1, 2, 3, 4

[43] Gui-Song Xia, Xiang Bai, Jian Ding, Zhen Zhu, Serge Belongie, Jiebo Luo, Mihai Datcu, Marcello Pelillo, and Liangpei Zhang. Dota: A large-scale dataset for object detection in aerial images. In *Proceedings of the IEEE Conference on Computer Vision and Pattern Recognition*, pages 3974–3983, 2018. 1

[44] Gui-Song Xia, Jingwen Hu, Fan Hu, Baoguang Shi, Xiang Bai, Yanfei Zhong, Liangpei Zhang, and Xiaoqiang Lu. Aid: A benchmark data set for performance evaluation of aerial scene classification. *IEEE Transactions on Geoscience and Remote Sensing*, 55(7):3965–3981, 2017. 1

[45] Shaokang Yang, Shuai Liu, Cheng Yang, and Changhu Wang. Re-rank coarse classification with local region enhanced features for fine-grained image recognition. *arXiv preprint arXiv:2102.09875*, 2021. 1, 6

[46] Sangdoo Yun, Dongyoon Han, Seong Joon Oh, Sanghyuk Chun, Junsuk Choe, and Youngjoon Yoo. Cutmix: Regularization strategy to train strong classifiers with localizable features. In *Proceedings of the IEEE/CVF International Conference on Computer Vision*, pages 6023–6032, 2019. 2, 5, 11, 12

[47] Hongyi Zhang, Moustapha Cisse, Yann N. Dauphin, and David Lopez-Paz. mixup: Beyond empirical risk minimization. In *International Conference on Learning Representations*, 2018. 2, 5, 11, 12

[48] Heliang Zheng, Jianlong Fu, Tao Mei, and Jiebo Luo. Learning multi-attention convolutional neural network for fine-grained image recognition. In *Proceedings of the IEEE international conference on computer vision*, pages 5209–5217, 2017. 1, 6

[49] Xiao Xiang Zhu, Devis Tuia, Lichao Mou, Gui-Song Xia, Liangpei Zhang, Feng Xu, and Friedrich Fraundorfer. Deep learning in remote sensing: A comprehensive review and list of resources. *IEEE Geoscience and Remote Sensing Magazine*, 5(4):8–36, 2017. 1

A. Hyperparameters of the methods

In Tab. 4 we list the candidate values and final determined values for each method’s hyperparameters. We make a few notes on the meaning of each symbol. For ODIN and Energy, τ is the temperature factor used to scale the model logits. Note, we do not use input pre-processing for ODIN as it is known that the perturbation hyperparameter may need exact test OOD distribution to tune [13, 15], and ODIN’s performance is largely attributed to the temperature scaling rather than the pre-processing [34]. For Rotation and OE, β is the weighting term that controls the contribution of their regularization objective. For Corruption, γ is the probability that corrupted data are used at each step of the training. For EnergyOE, m_{in} and m_{out} is the energy threshold for ID and training outlier data, respectively. We use $\beta = 0.1$ for EnergyOE, as we find that a larger β can hurt ID accuracy. For Mix and MixOE training, β again weights the regularization strength (see Eq. (2)). α is used to parameterize the Beta distribution for the mixing operations.

Table 4. The candidate values and final determined values for the hyperparameters of each method.

	Aircraft		Car		Butterfly		Bird	
	Candidates	Determined	Candidates	Determined	Candidates	Determined	Candidates	Determined
ODIN [26]	$\tau = \{10, 100, 1000\}$	$\tau = 1000$	$\tau = \{10, 100, 1000\}$	$\tau = 1000$	$\tau = \{10, 100, 1000\}$	$\tau = 1000$	$\tau = \{10, 100, 1000\}$	$\tau = 1000$
Energy [27]	$\tau = \{1, 10, 100\}$	$\tau = 1$	$\tau = \{1, 10, 100\}$	$\tau = 1$	$\tau = \{1, 10, 100\}$	$\tau = 1$	$\tau = \{1, 10, 100\}$	$\tau = 1$
Rotation [1]	$\beta = \{0.5, 1.0\}$	$\beta = 1.0$	$\beta = \{0.5, 1.0\}$	$\beta = 1.0$	$\beta = \{0.5, 1.0\}$	$\beta = 1.0$	$\beta = \{0.5, 1.0\}$	$\beta = 1.0$
Corruption [37]	$\gamma = \{0.2, 0.4\}$	$\beta = 0.2$	$\gamma = \{0.2, 0.4\}$	$\beta = 0.2$	$\gamma = \{0.2, 0.4\}$	$\beta = 0.2$	$\gamma = \{0.2, 0.4\}$	$\beta = 0.2$
OE [13]	$\beta = \{0.5, 1.0, 5.0\}$	$\beta = 1.0$	$\beta = \{0.5, 1.0, 5.0\}$	$\beta = 1.0$	$\beta = \{0.5, 1.0, 5.0\}$	$\beta = 1.0$	$\beta = \{0.5, 1.0, 5.0\}$	$\beta = 1.0$
EnergyOE [27]	$m_{in} = \{-9, -13, -17\}$ $m_{out} = \{-5, -7, -9\}$	$m_{in} = -17$ $m_{out} = -9$	$m_{in} = \{-9, -13, -17\}$ $m_{out} = \{-4, -6, -8\}$	$m_{in} = -13$ $m_{out} = -6$	$m_{in} = \{-10, -14, -18\}$ $m_{out} = \{-5, -7, -9\}$	$m_{in} = -14$ $m_{out} = -5$	$m_{in} = \{-9, -13, -17\}$ $m_{out} = \{-5, -7, -9\}$	$m_{in} = -13$ $m_{out} = -5$
Mix-linear [47]	$\alpha = \{0.4, 1.0, 2.0\}$ $\beta = \{0.5, 1.0, 5.0\}$	$\alpha = 1.0$ $\beta = 1.0$	$\alpha = \{0.4, 1.0, 2.0\}$ $\beta = \{0.5, 1.0, 5.0\}$	$\alpha = 2.0$ $\beta = 5.0$	$\alpha = \{0.4, 1.0, 2.0\}$ $\beta = \{0.5, 1.0, 5.0\}$	$\alpha = 1.0$ $\beta = 0.5$	$\alpha = \{0.4, 1.0, 2.0\}$ $\beta = \{0.5, 1.0, 5.0\}$	$\alpha = 1.0$ $\beta = 0.5$
Mix-cut [46]	$\alpha = \{0.4, 1.0, 2.0\}$ $\beta = \{0.5, 1.0, 5.0\}$	$\alpha = 2.0$ $\beta = 5.0$	$\alpha = \{0.4, 1.0, 2.0\}$ $\beta = \{0.5, 1.0, 5.0\}$	$\alpha = 2.0$ $\beta = 5.0$	$\alpha = \{0.4, 1.0, 2.0\}$ $\beta = \{0.5, 1.0, 5.0\}$	$\alpha = 0.4$ $\beta = 0.5$	$\alpha = \{0.4, 1.0, 2.0\}$ $\beta = \{0.5, 1.0, 5.0\}$	$\alpha = 0.4$ $\beta = 0.5$
MixOE-linear	$\alpha = \{0.4, 1.0, 2.0\}$ $\beta = \{0.5, 1.0, 5.0\}$	$\alpha = 1.0$ $\beta = 5.0$	$\alpha = \{0.4, 1.0, 2.0\}$ $\beta = \{0.5, 1.0, 5.0\}$	$\alpha = 1.0$ $\beta = 5.0$	$\alpha = \{0.4, 1.0, 2.0\}$ $\beta = \{0.5, 1.0, 5.0\}$	$\alpha = 1.0$ $\beta = 5.0$	$\alpha = \{0.4, 1.0, 2.0\}$ $\beta = \{0.5, 1.0, 5.0\}$	$\alpha = 1.0$ $\beta = 5.0$
MixOE-cut	$\alpha = \{0.4, 1.0, 2.0\}$ $\beta = \{0.5, 1.0, 5.0\}$	$\alpha = 2.0$ $\beta = 5.0$	$\alpha = \{0.4, 1.0, 2.0\}$ $\beta = \{0.5, 1.0, 5.0\}$	$\alpha = 2.0$ $\beta = 5.0$	$\alpha = \{0.4, 1.0, 2.0\}$ $\beta = \{0.5, 1.0, 5.0\}$	$\alpha = 1.0$ $\beta = 5.0$	$\alpha = \{0.4, 1.0, 2.0\}$ $\beta = \{0.5, 1.0, 5.0\}$	$\alpha = 1.0$ $\beta = 5.0$

B. Visualization procedure

Following [30], the visualization is enabled by training a “visualization” layer (denoted as vis layer for brevity). Specifically, the vis layer is a fully-connected layer that maps the output of DNN’s penultimate layer (in our case with ResNet-50 the dimension is 2048) to a 2D space. When training such vis layer, we concatenate it to the penultimate layer of the ResNet and add another consequent linear layer that maps the 2D output of the vis layer to the class logits. The vis layer is then trained by minimizing the standard cross-entropy loss on the ID training data. Note, during the training the parameters of the DNN model is freezed, so the visualization is faithful to the model. After the training is completed, the visualization is performed by forward passing inputs into the model and taking the 2D outputs of the vis layer.

C. Additional plots and results

Here we provide additional plots and results that are not shown in the main document due to space limit. Table 5 presents the full detection results in terms of both TNR95 and AUROC for all methods on all splits/datasets. Figure 8 includes the bar plots that visualize the TNR95 statistics of existing methods on all splits/datasets. The corresponding numerical results can be found in Tab. 5. Figures 9 to 12 show the confidence distributions of the Standard, OE, Corruption, Mix, and MixOE models on all splits/datasets. Figures 13 to 16 show the 2D visualization of ID/OOD/training outlier data using all datasets. Table 6 presents the accuracy results of all methods on all splits/datasets.

Table 5. Full detection results. The number before and after the slash is for coarse-grained and fine-grained OOD samples, respectively. Avg. diff. is the average difference (across three splits) relative to MSP.

\mathcal{D}_{in}	Method	Split 1		Split 2		Split 3		Avg. diff.	
		TNR95	AUROC	TNR95	AUROC	TNR95	AUROC	TNR95	AUROC
Aircraft	MSP [12]	75.0 / 29.9	95.6 / 85.9	61.6 / 15.9	93.6 / 78.7	77.1 / 18.5	95.8 / 77.6	- / -	- / -
	ODIN [26]	87.5 / 30.2	97.4 / 85.5	73.2 / 15.3	95.6 / 75.5	86.5 / 15.8	97.2 / 78.6	+11.2 / -1.0	+1.7 / -0.9
	Energy [27]	88.5 / 30.1	97.5 / 85.2	74.4 / 14.6	95.6 / 74.9	86.2 / 16.3	97.2 / 78.3	+11.8 / -1.1	+1.8 / -1.3
	Rotation [1]	65.5 / 31.4	94.0 / 86.0	55.0 / 15.9	92.2 / 79.1	65.5 / 17.6	93.4 / 77.6	-9.2 / +0.2	-1.8 / +0.2
	Corruption [37]	95.9 / 33.2	99.2 / 87.2	94.2 / 20.1	98.9 / 81.1	95.6 / 19.4	99.0 / 76.9	+24.0 / +2.8	+4.0 / +1.0
	OE [13]	99.3 / 27.8	99.8 / 84.6	98.5 / 16.0	99.6 / 78.4	98.7 / 16.5	99.7 / 78.7	+27.6 / -1.3	+4.7 / -0.2
	EnergyOE [27]	99.8 / 30.3	99.9 / 86.9	99.7 / 17.0	99.8 / 76.7	99.7 / 19.9	99.8 / 79.1	+28.5 / +1.0	+4.8 / +0.2
	Mix-linear [47]	80.6 / 34.2	96.2 / 86.6	80.5 / 19.8	96.6 / 77.6	76.8 / 20.9	95.6 / 78.4	+8.1 / +3.5	+1.1 / +0.1
	Mix-cut [46]	68.1 / 33.6	94.3 / 86.6	63.1 / 24.3	92.9 / 78.0	70.1 / 16.9	94.9 / 77.4	-4.1 / +3.5	-1.0 / -0.1
	MixOE-linear	93.2 / 41.4	98.3 / 89.5	88.4 / 24.6	97.9 / 81.8	92.1 / 16.5	98.3 / 80.9	+20.0 / +6.1	+3.2 / +3.3
	MixOE-cut	99.0 / 39.8	99.7 / 89.4	99.4 / 23.7	99.7 / 80.1	99.4 / 24.9	99.8 / 78.6	+28.0 / +8.0	+4.7 / +2.0
Car	MSP [12]	95.5 / 58.5	98.8 / 90.2	88.0 / 56.3	97.8 / 90.6	78.8 / 53.5	96.4 / 90.2	- / -	- / -
	ODIN [26]	99.6 / 55.6	99.7 / 89.0	99.1 / 47.0	99.5 / 88.2	97.8 / 49.0	99.2 / 88.7	+11.4 / -5.6	+1.8 / -1.7
	Energy [27]	99.7 / 49.1	99.8 / 88.1	99.4 / 39.7	99.7 / 86.8	99.1 / 42.6	99.6 / 87.7	+12.0 / -12.3	+2.0 / -2.8
	Rotation [1]	97.7 / 58.9	99.3 / 90.5	88.1 / 52.4	97.6 / 90.1	81.3 / 50.4	96.9 / 90.0	+1.6 / -2.2	+0.3 / -0.1
	Corruption [37]	99.5 / 63.0	99.9 / 91.0	99.2 / 55.5	99.8 / 90.4	98.2 / 60.0	99.7 / 91.5	+11.5 / +3.4	+2.1 / +0.6
	OE [13]	99.9 / 53.2	100.0 / 89.9	100.0 / 53.0	100.0 / 89.7	99.9 / 51.2	100.0 / 90.2	+12.5 / -3.6	+2.3 / -0.4
	EnergyOE [27]	100.0 / 52.6	100.0 / 89.0	100.0 / 41.0	100.0 / 87.2	100.0 / 44.9	100.0 / 88.3	+12.6 / -9.9	+2.3 / -2.2
	Mix-linear [47]	95.9 / 66.3	98.8 / 91.9	82.6 / 52.3	96.7 / 89.0	77.8 / 58.6	95.5 / 91.2	-2.0 / +3.0	-0.7 / +0.4
	Mix-cut [46]	84.6 / 68.8	97.0 / 92.0	70.6 / 65.3	93.8 / 92.2	70.6 / 61.6	93.1 / 91.6	-12.2 / +9.1	-3.0 / +1.6
	MixOE-linear	99.6 / 65.9	99.8 / 92.2	99.7 / 62.9	99.8 / 92.3	99.5 / 60.1	99.8 / 92.0	+12.2 / +6.9	+2.1 / +1.8
	MixOE-cut	99.9 / 70.3	99.9 / 92.6	100.0 / 69.8	99.9 / 93.0	99.9 / 66.5	99.9 / 93.1	+12.5 / +12.8	+2.2 / +2.6
Butterfly	MSP [12]	87.1 / 29.9	97.8 / 79.3	89.9 / 31.8	97.9 / 78.2	88.4 / 36.6	97.9 / 83.8	- / -	- / -
	ODIN [26]	95.2 / 28.2	98.7 / 74.5	95.5 / 32.5	98.8 / 77.3	95.6 / 38.7	98.8 / 82.5	+7.0 / +0.4	+0.9 / -2.3
	Energy [27]	95.3 / 25.5	98.7 / 73.9	95.2 / 30.2	98.7 / 76.7	95.6 / 36.1	98.7 / 82.0	+6.9 / -2.2	+0.8 / -2.9
	Rotation [1]	87.9 / 27.6	97.8 / 78.0	88.5 / 31.2	97.9 / 79.7	86.2 / 37.0	97.5 / 83.9	-0.9 / -0.8	-0.1 / +0.1
	Corruption [37]	94.1 / 29.0	98.8 / 79.5	94.2 / 32.9	98.7 / 80.4	92.1 / 38.0	98.5 / 84.2	+5.0 / +0.5	+0.8 / +0.9
	OE [13]	92.2 / 26.5	98.4 / 77.8	93.7 / 32.1	98.4 / 79.3	94.3 / 34.3	98.6 / 82.6	+4.9 / -1.8	+0.6 / -0.5
	EnergyOE [27]	97.8 / 25.1	99.1 / 73.5	96.9 / 30.5	98.9 / 75.9	98.2 / 37.2	99.1 / 82.6	+9.2 / -1.8	+1.2 / -3.1
	Mix-linear [47]	90.7 / 31.3	98.1 / 78.5	88.7 / 34.9	97.8 / 80.6	84.7 / 37.9	97.2 / 83.6	-0.4 / +1.9	-0.2 / +0.5
	Mix-cut [46]	85.7 / 30.4	97.3 / 78.6	86.3 / 34.6	97.2 / 79.7	84.7 / 40.5	97.1 / 84.3	-2.9 / +2.4	-0.7 / +0.4
	MixOE-linear	95.3 / 32.6	98.7 / 78.3	93.9 / 37.9	98.6 / 80.9	95.5 / 45.0	98.8 / 84.9	+6.4 / +5.7	+0.8 / +0.9
	MixOE-cut	94.9 / 35.8	98.8 / 79.8	94.1 / 38.8	98.7 / 81.7	92.7 / 46.0	98.6 / 86.8	+5.4 / +7.4	+0.8 / +2.3
Bird	MSP [12]	72.3 / 22.6	93.7 / 76.4	67.4 / 22.3	93.5 / 78.0	66.4 / 22.3	92.9 / 76.9	- / -	- / -
	ODIN [26]	80.9 / 22.7	95.3 / 75.5	77.2 / 21.5	95.5 / 76.6	74.3 / 21.9	94.5 / 75.8	+8.8 / -0.4	+1.7 / -1.1
	Energy [27]	80.8 / 20.3	95.3 / 74.8	76.5 / 18.4	95.4 / 75.5	73.9 / 18.8	94.4 / 74.8	+8.4 / -3.2	+1.7 / -2.1
	Rotation [1]	71.3 / 23.6	93.9 / 76.0	64.0 / 24.0	92.7 / 78.7	65.4 / 21.5	92.8 / 76.8	-1.8 / +0.6	-0.2 / +0.1
	Corruption [37]	81.1 / 23.2	95.8 / 77.3	81.8 / 23.7	96.3 / 79.8	83.9 / 26.6	96.7 / 78.8	+13.6 / +2.1	+2.9 / +1.5
	OE [13]	98.2 / 20.6	99.5 / 75.9	97.9 / 22.9	99.5 / 78.2	97.9 / 20.7	99.5 / 77.0	+29.3 / -1.0	+6.1 / -0.1
	EnergyOE [27]	98.6 / 19.4	99.6 / 74.4	99.0 / 18.4	99.7 / 76.2	99.3 / 19.5	99.7 / 77.7	+30.3 / -3.3	+6.3 / -1.0
	Mix-linear [47]	72.1 / 24.4	94.0 / 77.6	70.0 / 25.3	94.0 / 79.9	71.0 / 25.0	94.3 / 79.5	+2.3 / +2.5	+0.7 / +1.9
	Mix-cut [46]	69.0 / 25.6	93.5 / 77.1	58.7 / 23.6	92.1 / 79.2	65.3 / 25.0	92.9 / 77.9	-4.4 / +2.3	-0.5 / +1.0
	MixOE-linear	88.6 / 24.9	97.6 / 77.8	83.9 / 26.7	96.6 / 80.6	86.3 / 28.6	97.1 / 80.7	+17.6 / +4.3	+3.7 / +2.6
	MixOE-cut	91.0 / 27.7	98.0 / 78.6	91.8 / 24.6	98.4 / 80.2	92.9 / 27.7	98.7 / 80.0	+23.2 / +4.3	+5.0 / +2.5

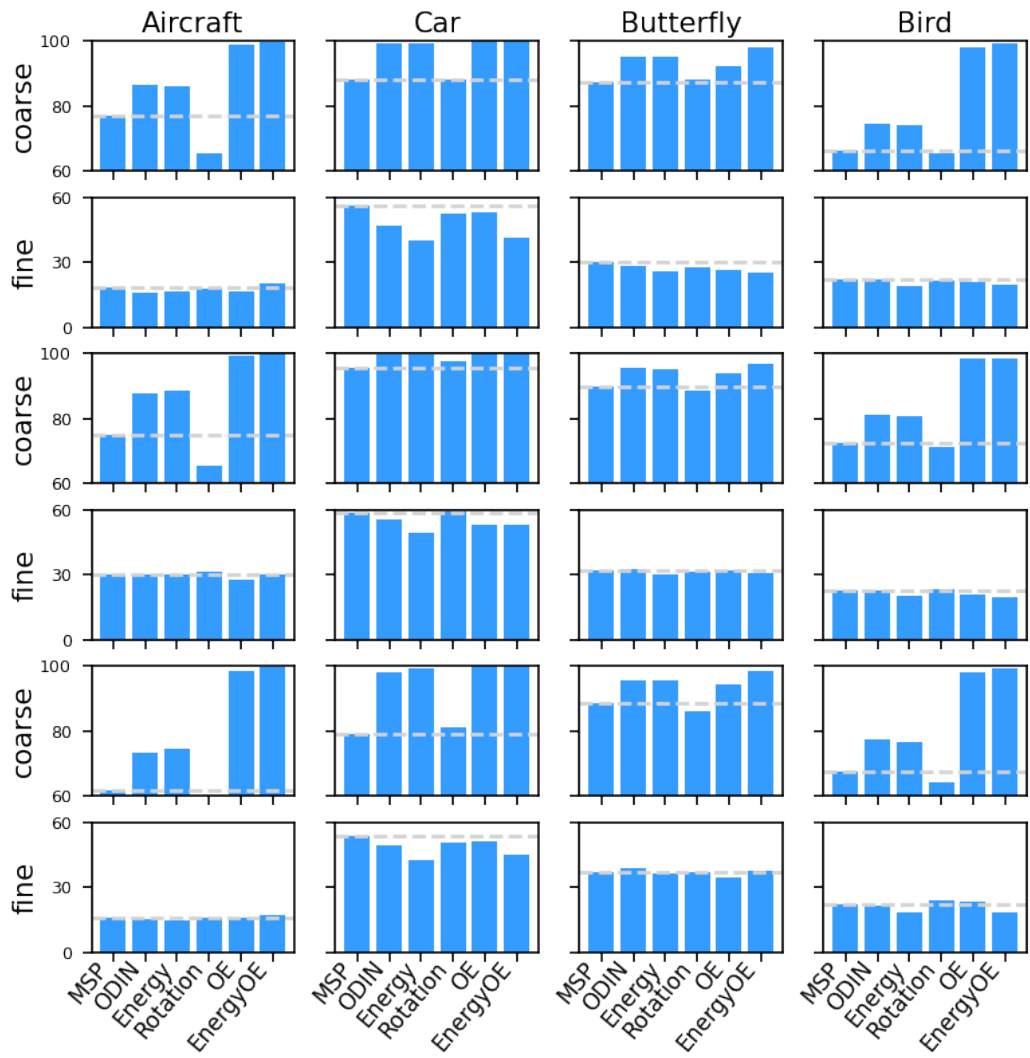


Figure 8. TNR95 statistics of existing methods on all of the three splits in each dataset. Each two rows correspond to one split.

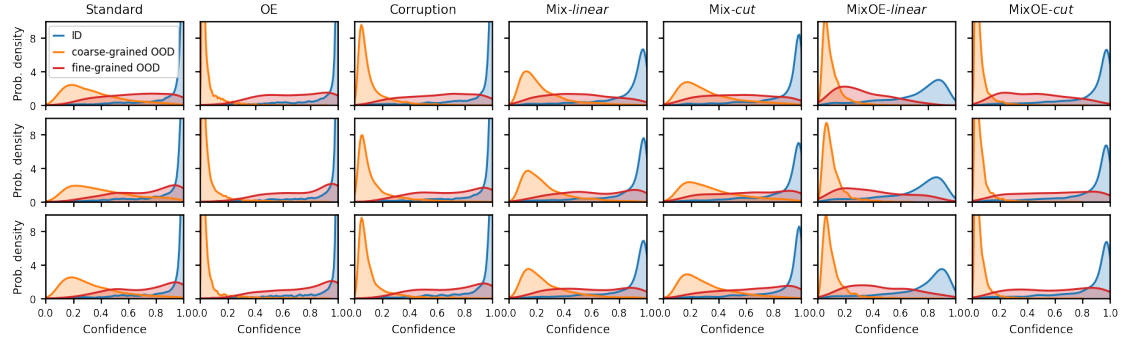


Figure 9. Confidence density plots on the three splits in the *Aircraft* dataset.

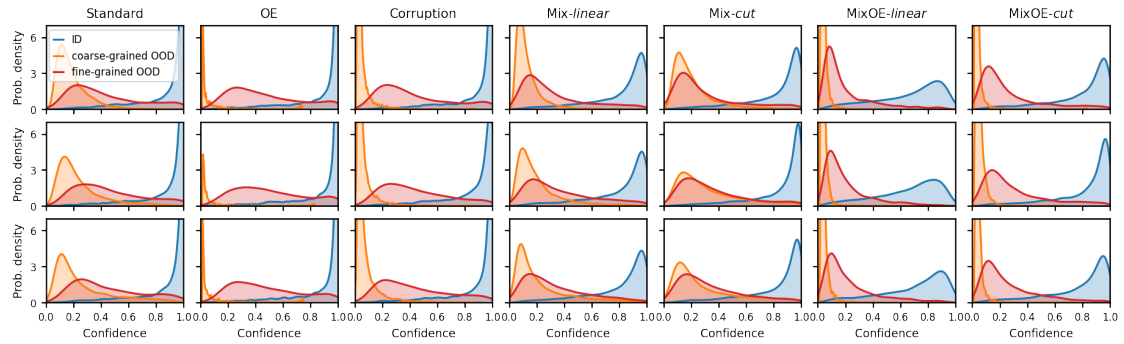


Figure 10. Confidence density plots on the three splits in the *Car* dataset.

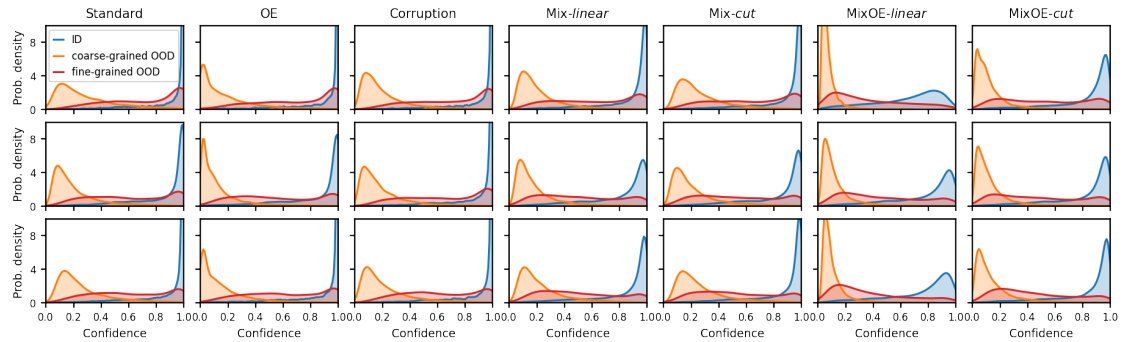


Figure 11. Confidence density plots on the three splits in the *Butterfly* dataset.

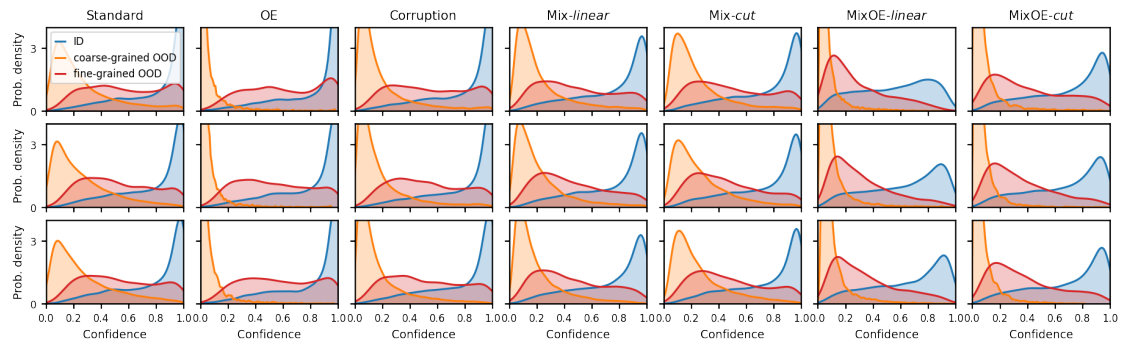


Figure 12. Confidence density plots on the three splits in the *Bird* dataset.

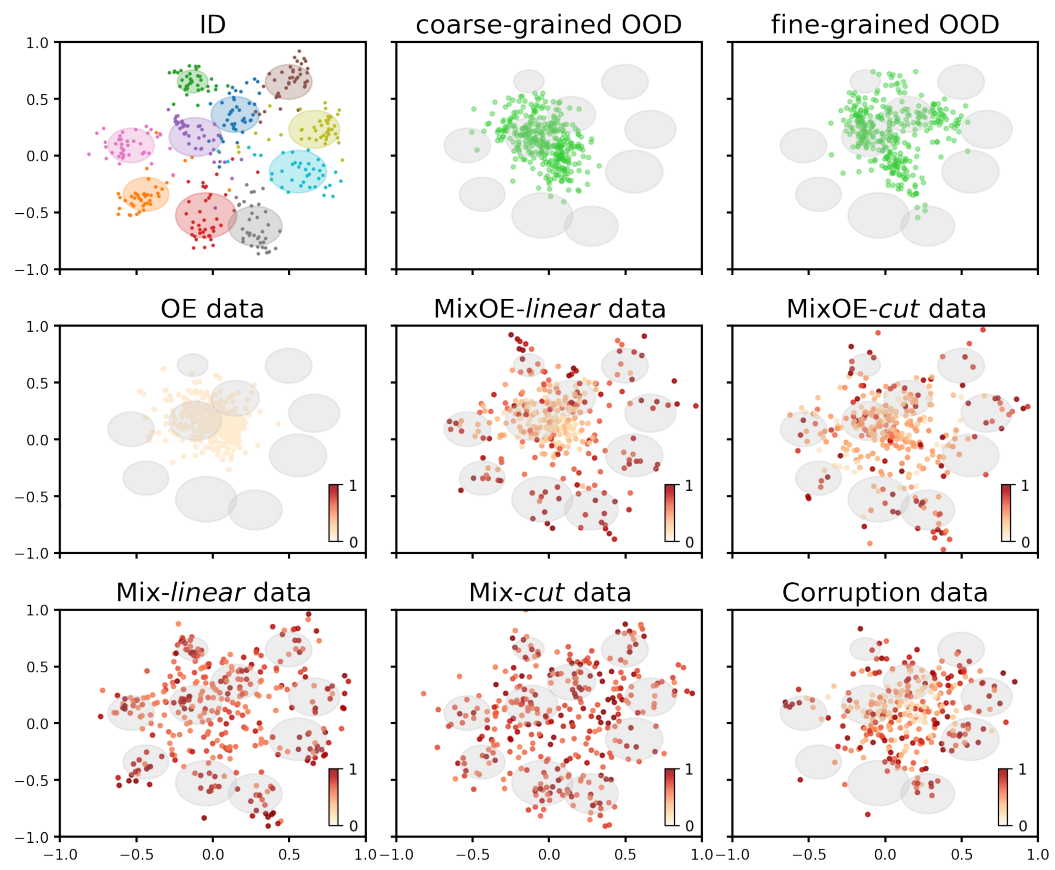


Figure 13. 2D visualization of ID/OOD/training outlier data in the feature space for the *Aircraft* dataset.

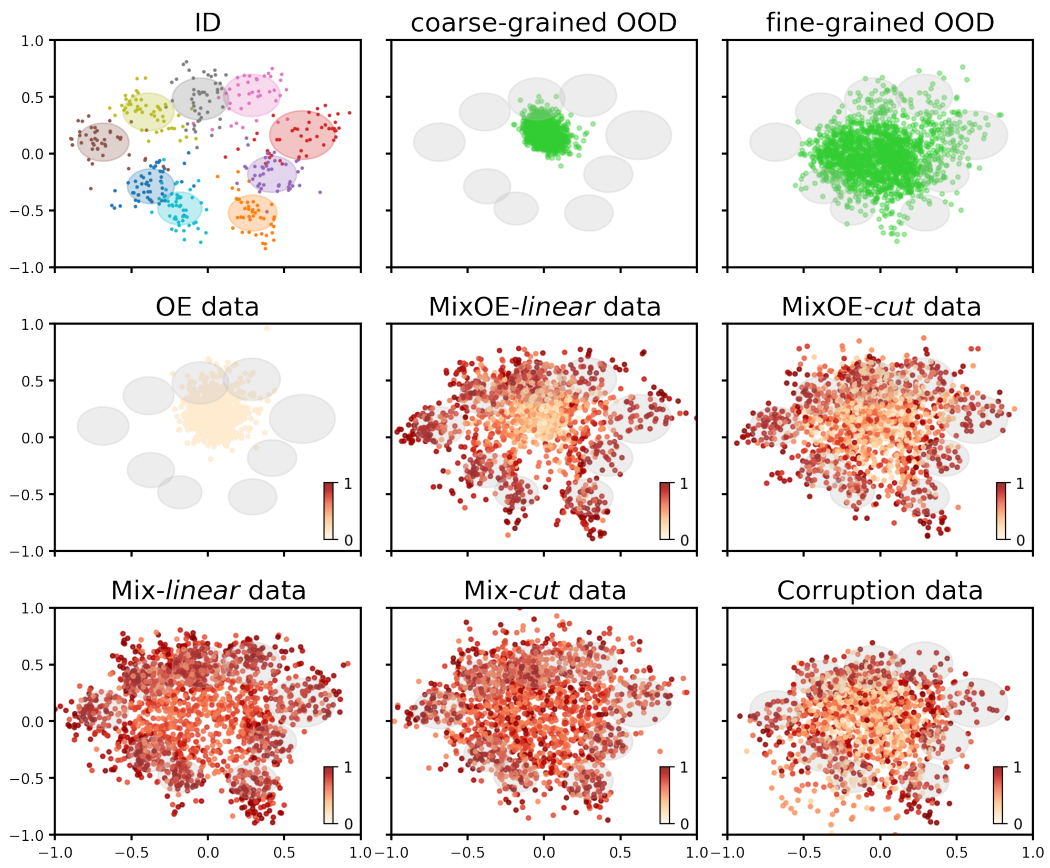


Figure 14. 2D visualization of ID/OOD/training outlier data in the feature space for the *Car* dataset.

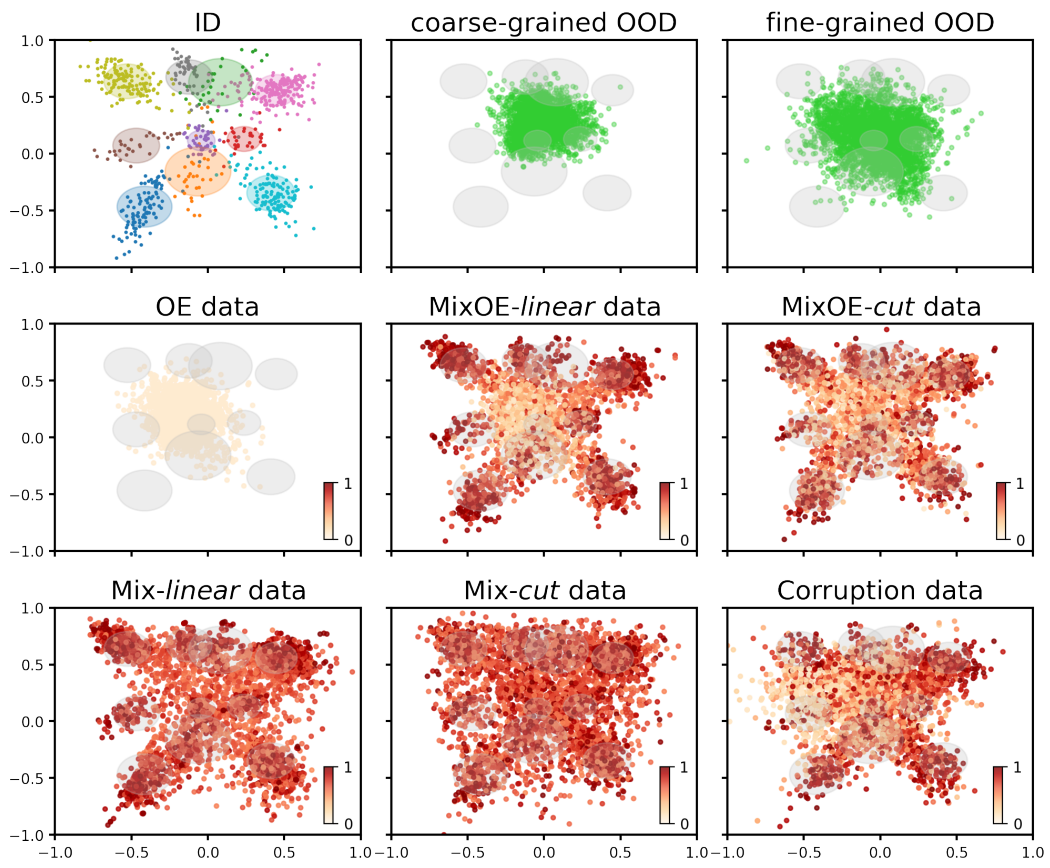


Figure 15. 2D visualization of ID/OOD/training outlier data in the feature space for the *Butterfly* dataset.

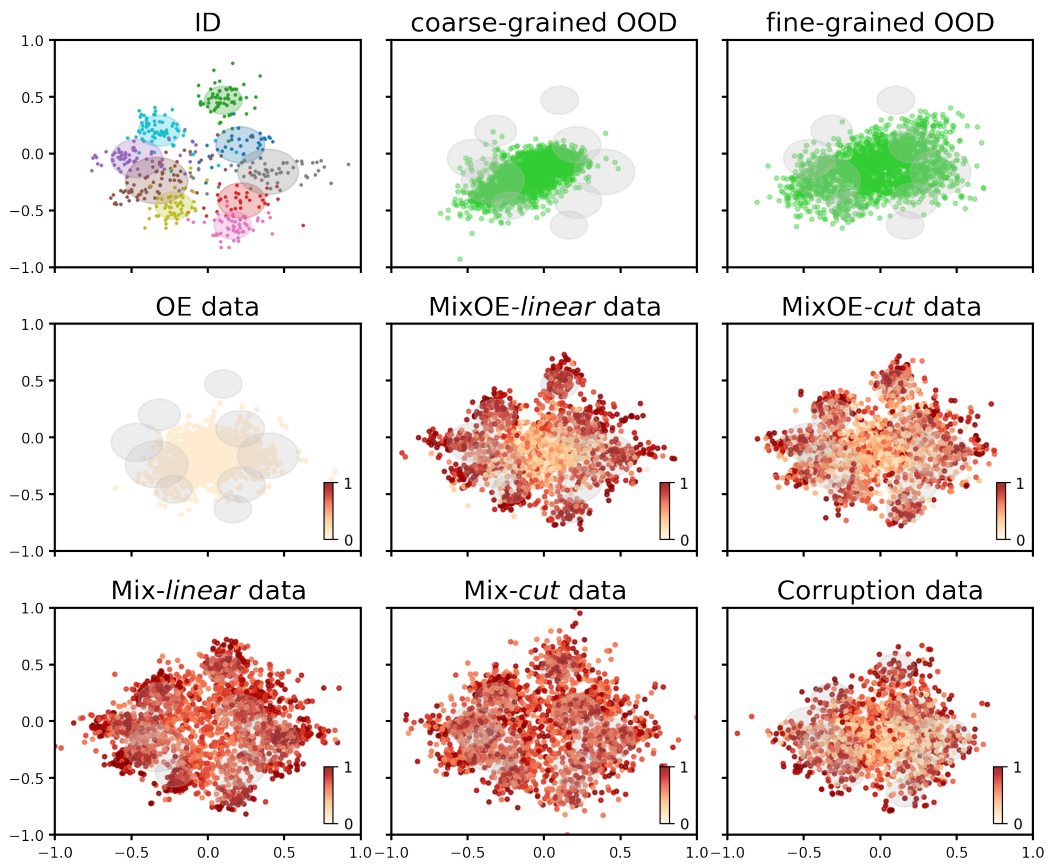


Figure 16. 2D visualization of ID/OOD/training outlier data in the feature space for the *Bird* dataset.

Table 6. Full accuracy results on each split of each dataset.

\mathcal{D}_{in}	Method	Split 1	Split 2	Split 3
Aircraft	Standard	89.53	89.41	89.94
	Rotation [1]	88.20	88.31	89.01
	Corruption [37]	90.03	89.77	89.54
	OE [13]	88.57	88.87	90.08
	EnergyOE [27]	89.27	88.81	89.88
	MixOE- <i>linear</i>	89.93	90.81	90.64
	MixOE- <i>cut</i>	89.77	90.21	90.31
Car	Standard	91.74	92.19	91.57
	Rotation [1]	91.38	91.64	90.82
	Corruption [37]	92.61	92.32	92.32
	OE [13]	91.56	91.75	91.53
	EnergyOE [27]	91.61	92.16	91.76
	MixOE- <i>linear</i>	92.53	93.53	92.76
	MixOE- <i>cut</i>	92.74	93.46	92.56
Butterfly	Standard	90.21	87.28	89.38
	Rotation [1]	89.75	87.88	88.88
	Corruption [37]	90.69	88.49	89.56
	OE [13]	89.74	86.13	88.41
	EnergyOE [27]	90.21	87.22	88.86
	MixOE- <i>linear</i>	90.71	88.04	89.10
	MixOE- <i>cut</i>	91.33	88.46	90.53
Bird	Standard	83.30	82.03	80.96
	Rotation [1]	82.47	82.25	81.26
	Corruption [37]	84.42	83.82	82.84
	OE [13]	83.32	82.03	81.75
	EnergyOE [27]	82.89	82.57	81.36
	MixOE- <i>linear</i>	84.18	83.29	82.75
	MixOE- <i>cut</i>	84.37	83.44	82.57